
Generalized Spectral Mixture Kernels for Multi-Task Gaussian Processes

Kai Chen

Shenzhen Institutes of Advanced Technology, Chinese Academy of Sciences
Shenzhen College of Advanced Technology, University of Chinese Academy of Sciences
Institute for Computing and Information Sciences, Radboud University
kchen@cs.ru.nl

Perry Groot

Institute for Computing and Information Sciences, Radboud University
perry.groot@science.ru.nl

Jinsong Chen

Shenzhen Institutes of Advanced Technology, Chinese Academy of Sciences
js.chen@siat.ac.cn

Elena Marchiori

Institute for Computing and Information Sciences, Radboud University
elenam@cs.ru.nl

Abstract

Multi-Task Gaussian processes (MTGPs) have shown a significant progress both in expressiveness and interpretation of the relatedness between different tasks: from linear combinations of independent single-output Gaussian processes (GPs), through the direct modeling of the cross-covariances such as spectral mixture kernels with phase shift, to the design of multivariate covariance functions based on spectral mixture kernels which model delays among tasks in addition to phase differences, and which provide a parametric interpretation of the relatedness across tasks. In this paper we further extend expressiveness and interpretability of MTGPs models and introduce a new family of kernels capable to model nonlinear correlations between tasks as well as dependencies between component, including time and phase delay. Specifically, we use generalized convolution spectral mixture kernels for modeling dependencies at component level, and coupling coregionalization for discovering task level correlations. The proposed kernels for MTGP are validated on artificial data and compared with existing MTGPs methods on three real-world experiments. Results indicate the benefits of our more expressive representation with respect to performance and interpretability.

1 Introduction

Gaussian processes (GPs) [1, 2] are an elegant Bayesian approach to model an unknown function. They provide regression models where a posterior distribution over the unknown function is maintained as evidence is accumulated. This allows GPs to learn complex functions if a large amount of evidence is available and makes them robust against overfitting in the presence of little evidence. A GP can model a large class of phenomena through the choice of its kernel which characterizes

one’s assumption on how the unknown function autocovaries [1]. The choice of kernel is a core aspect of GP design, since the posterior distribution can significantly vary for different kernels. As a consequence, various kernels, e.g. Squared Exponential, Periodic, Matérn, and kernel design methods have been proposed [2]. The extension of GPs to multiple sources of data is known as multi-task Gaussian processes (MTGPs) [3]. MTGPs model temporal or spatial relationships among infinitely many random variables, as scalar GPs, but also account for the statistical dependence across different sources of data (or tasks) [3, 4, 5, 6, 7, 8, 9]. How to choose an appropriate kernel to jointly model the cross covariance between tasks and auto-covariance within each task is the core aspect of MTGPs design [3, 10, 11, 12, 5, 13, 14].

Early approaches to MTGPs, like Linear Model of Coregionalization (LMC [15] [4] [8]), focused on linear combination of independent single-output GPs. More expressive methods like the multi-kernel method [12] and the convolved latent function framework [16, 17, 18, 19] consider convolution to construct cross-covariance function, and assume that each task has its own kernel. The use of spectral mixture (SM) kernels has further boosted the development of MTGP methods. Specifically, the expressiveness power of MTGP methods with SM kernels has increased during the past years: first the SM-LMC kernel was proposed [20, 21], which just uses independent component; then the Cross-Spectral Mixture (CSM) kernel [22], a more flexible kernel which considers the power and phase correlation between multiple tasks. CSM cannot capture complicated cross correlations because it only considers phase dependencies between tasks. Therefore the Multi-Output Spectral Mixture kernel (MOSM) was proposed [23] which addresses this limitation. However, MOSM considers task level correlations within each component by using independent components.

We propose a more expressive and interpretable kernel for MTGPs which is capable to model nonlinear correlations between tasks and dependencies between component. Such correlations and dependencies model more complex patterns in multi-source data and more expressive characteristics of latent functions. By using generalized convolution spectral mixture kernel (GCSM) [24], our kernel is able to model dependencies between component including time and phase delay. Task level correlations are modeled through coupling coregionalization, providing a strong interpretation of relations between tasks. Furthermore, when applied to a single task, the proposed kernel reduces to GCSM, which has been shown to be a generalization of the ordinary SM kernel. The proposed MTGP kernel is more expressive than existing ones because it explicitly models correlations at task and component level. These modeling capabilities are comparatively investigated on artificial data and on four real-world experiments.

The rest of the paper is organized as follows. In the next section GPs, spectral mixture kernels, and existing multitask GPs are described. In Section 3 our kernel for MTGPs is introduced and compared with existing methods. Experiments on artificial and real-world data are described in Section 4. We conclude with a summary of our contributions and future work.

2 Background

We start with some background information on GPs, multi-task GPs, and spectral mixture kernels.

2.1 Gaussian processes

A Gaussian process defines a distribution over functions, specified by its mean function $m(\mathbf{x})$ and covariance function $k(\mathbf{x}, \mathbf{x}')$ [2] for given input vector $\mathbf{x} \in \mathbb{R}^P$. Thus we can define a GP as

$$f(\mathbf{x}) \sim \mathcal{GP}(m(\mathbf{x}), k(\mathbf{x}, \mathbf{x}')) \quad (1)$$

Without loss of generality we assume the mean of a GP to be zero. The covariance function is applied to construct a positive definite covariance matrix on input points X , here denoted by $K = K(X, X)$. By placing a GP prior over functions through the choice of a kernel and parameter initialization, from the training data X we can predict the unknown function value \tilde{y}_* and its variance $\mathbb{V}[y_*]$ (that is, its uncertainty) for a test point \mathbf{x}_* using the following key predictive equations for GP regression [2]:

$$\tilde{y}_* = \mathbf{k}_*^\top (K + \sigma_n^2 I)^{-1} \mathbf{y} \quad (2)$$

$$\mathbb{V}[y_*] = k(\mathbf{x}_*, \mathbf{x}_*) - \mathbf{k}_*^\top (K + \sigma_n^2 I)^{-1} \mathbf{k}_* \quad (3)$$

where \mathbf{k}_*^\top is the covariances vector between \mathbf{x}_* and X , and \mathbf{y} are the observed values corresponding to X . Typically, GPs contain free parameters Θ , called hyper-parameters, which can be optimized by

minimizing the Negative Log Marginal Likelihood (NLML) as follows:

$$\begin{aligned} \text{NLML} &= -\log p(\mathbf{y}|\mathbf{x}, \Theta) \\ &\propto \underbrace{\frac{1}{2}\mathbf{y}^\top (K + \sigma_n^2 I)^{-1} \mathbf{y}}_{\text{model fit}} + \underbrace{\frac{1}{2} \log |K + \sigma_n^2 I|}_{\text{complexity penalty}} \end{aligned} \quad (4)$$

where σ_n^2 is the noise level. This formulation follows directly from the fact that $\mathbf{y} \sim \mathcal{N}(0, K + \sigma_n^2 I)$.

In multi-task GP (MTGP), we have multiple sources of data which specify related tasks [3, 7, 10, 18]. The construction of the MTGP covariance function k_{MTGP} models dependencies between pairs of points from two tasks.

2.2 Spectral mixture kernels

The smoothness and generalization properties of GPs depend on the kernel function and its hyper-parameters Θ . Choosing an appropriate kernel function and its initial hyper-parameters based on prior knowledge from the data are the core steps of a GP. Various kernel functions have been proposed [2], such as Squared Exponential (SE), Periodic (PER), and general Matérn (MA). Recently new covariance kernels have been proposed in [20, 25], called Spectral Mixture (SM) kernels. An SM kernel, here denoted by k_{SM} , is derived through modeling spectral densities (Fourier transform of a kernel) with Gaussian mixture. A desirable property of SM kernels is that they can be used to reconstruct other popular standard covariance kernels. According to Bochner's Theorem [26], the properties of a stationary kernel entirely depend on its spectral densities. With enough components k_{SM} can approximate any stationary covariance kernel [25].

$$k_{\text{SM}}(\tau) = \sum_{i=1}^Q w_i k_{\text{SM}i}(\tau) \quad (5)$$

$$k_{\text{SM}i}(\tau) = \cos(2\pi\tau^\top \boldsymbol{\mu}_i) \prod_{p=1}^P \exp\left(-2\pi^2\tau^2 \Sigma_i^{(p)}\right) \quad (6)$$

where $\tau = \mathbf{x} - \mathbf{x}'$, Q is the number of components, $k_{\text{SM}i}$ is the i -th component, P is the dimension of input, w_i , $\boldsymbol{\mu}_i = [\mu_i^{(1)}, \dots, \mu_i^{(P)}]$, and $\Sigma_i = \text{diag}([\sigma_i^{(1)}, \dots, \sigma_i^{(P)}])$ are weight, mean, and variance of the i -th component in frequency domain, respectively. The variance σ_i^2 can be thought of as an inverse length-scale, μ_i as a frequency, and w_i as a contribution. Bochner's Theorem [26, 27] indicates a direction on how to construct a valid kernel from the frequency domain. We will use a hat $\hat{k}(\mathbf{s})$ to denote the spectral density of a covariance function $k(\tau)$ in the frequency domain. Using the following definition, the spectral density of kernel function $k(\tau)$ can be given by its Fourier transform:

$$\hat{k}(\mathbf{s}) = \int k(\tau) e^{-2\pi\tau\mathbf{s}i} d\tau \quad (7)$$

where i is the imaginary number. Furthermore, the inverse Fourier transform of spectral density $\hat{k}(\mathbf{s})$ is the original kernel function $k(\tau)$.

$$k(\tau) = \int \hat{k}(\mathbf{s}) e^{2\pi\tau\mathbf{s}i} d\mathbf{s} \quad (8)$$

For SM kernel [20], using inverse Fourier transform of the spectral density $\hat{k}_{\text{SM}i}(\mathbf{s}) = [\varphi_{\text{SM}i}(\mathbf{s}) + \varphi_{\text{SM}i}(-\mathbf{s})]/2$ where $\varphi_{\text{SM}i}(\mathbf{s}) = \mathcal{N}(\mathbf{s}; \boldsymbol{\mu}_i, \Sigma_i)$ is a symmetrized scale-location Gaussian in the frequency domain, we have

$$\begin{aligned} k_{\text{SM}}(\tau) &= \mathcal{F}_{\mathbf{s} \rightarrow \tau}^{-1} \left[\sum_{i=1}^Q w_i \hat{k}_{\text{SM}i}(\mathbf{s}) \right] (\tau) \\ &= \sum_{i=1}^Q w_i \mathcal{F}_{\mathbf{s} \rightarrow \tau}^{-1} [(\varphi_{\text{SM}i}(\mathbf{s}) + \varphi_{\text{SM}i}(-\mathbf{s}))/2] (\tau) \end{aligned} \quad (9)$$

where $\mathcal{F}_{\mathbf{s} \rightarrow \tau}^{-1}$ denotes inverse Fourier transform.

2.3 Existing MTGPs

Research on GPs related to multi-task learning include [4, 7, 8, 12, 13, 16, 28, 29, 30, 31, 32]. Here we mainly focus on MTGP methods based on spectral mixture kernels [21, 22, 23], because of their expressiveness and recent use in MTGPs. Since the introduction of SM kernels [25, 33], various MTGP methods have been introduced [33, 34, 35, 36, 37, 38]. The first MTGP using SM kernel is the Gaussian process regression network (GPRN), which based on the LMC framework [21].

$$K_{\text{SM-LMC}} = \sum_{i=1}^Q B_i \otimes K_{\text{SM}i}$$

The B_i in $K_{\text{SM-LMC}}$ encodes cross weights to represent task correlation and involves a linear combination of component. The CSM kernel [22] improved the expressivity of SM-LMC: it contains cross phase spectrum and is also defined within the LMC framework as

$$K_{\text{CSM}} = \sum_{i=1}^Q B_i k_{\text{SG}i}(\tau; \Theta^i)$$

where $k_{\text{SG}i}(\tau; \Theta^i)$ is phasor notation of the spectral Gaussian kernel. However the kernels $k_{\text{SG}i}(\tau; \Theta^i)$ used in the CSM are only phase dependent. The more recent MOSM kernel [23] provided a principled framework to construct multivariate covariance functions with a better interpretation of cross relationship between tasks. MOSM has the form

$$k_{\text{MOSM}}^{i \times j}(\tau) = \sum_{q=1}^Q \alpha_{ij}^q \exp\left(-\frac{1}{2}(\tau + \boldsymbol{\theta}_{ij}^q)^\top \Sigma_{ij}^q (\tau + \boldsymbol{\theta}_{ij}^q)\right) \cos\left((\tau + \boldsymbol{\theta}_{ij}^q)^\top \boldsymbol{\mu}_{ij}^q + \phi_{ij}^q\right)$$

where α_{ij}^q , Σ_{ij}^q , $\boldsymbol{\mu}_{ij}^q$, $\boldsymbol{\theta}_{ij}^q$, and ϕ_{ij}^q are cross magnitude, cross covariance, cross mean, cross time delay, and cross phase delay between the i -th and j -th channels. Here SM-LMC and CSM are instances of MOSM. Even if MOSM extend existing methods in expressiveness and interpretation, it still consider linear combination of components and it ignores dependencies between components. We address these two extensions in the proposed kernel described in the next section.

3 Generalized convolution spectral mixture of coupling coregionalization

In this section we address the following three questions. (1) How can we embed component level dependencies related to time and phase delay into coupling correlations between tasks over all components? (2) What is the interpretation of task level correlation (coupling coregionalization) and component dependency (convolution, time, and phase delay) in the proposed setting? (3) What is the difference between the proposed kernel and existing approaches to MTGPs?

3.1 Coupling coregionalization on component dependencies

We consider component level dependencies related to time and phase delay, as modeled in [24] through the so-called generalized convolution spectral mixture (GCSM) kernel, defined as follows:

$$\begin{aligned} k_{\text{GCSM}}(\tau) &= \mathcal{F}_{s \rightarrow \tau}^{-1} \left[\sum_{i=1}^Q \sum_{j=1}^Q \frac{1}{2} \left(\hat{k}_{\text{GCSM}}^{i \times j}(\mathbf{s}) + \hat{k}_{\text{GCSM}}^{i \times j}(-\mathbf{s}) \right) \right] (\tau) \\ &= \sum_{i=1}^Q \sum_{j=1}^Q w_{ij} a_{ij} \exp\left(-\frac{1}{2}\pi^2 (2\tau - \boldsymbol{\theta}_{ij})^\top \Sigma_{ij} (2\tau - \boldsymbol{\theta}_{ij})\right) \\ &\quad \times \cos\left(\pi \left((2\tau - \boldsymbol{\theta}_{ij})^\top \boldsymbol{\mu}_{ij} - \phi_{ij}\right)\right) \end{aligned} \quad (10)$$

where $w_{ij} a_{ij}$ is the cross contribution constant incorporating cross weight and cross amplitude. Other parameters are defined as:

- cross weight: $w_{ij} = \sqrt{w_i w_j}$

- cross amplitude: $a_{ij} = \left| \frac{\sqrt{4\Sigma_i\Sigma_j}}{\Sigma_i+\Sigma_j} \right|^{\frac{1}{2}} \exp\left(-\frac{1}{4}(\boldsymbol{\mu}_i - \boldsymbol{\mu}_j)^\top (\Sigma_i + \Sigma_j)^{-1}(\boldsymbol{\mu}_i - \boldsymbol{\mu}_j)\right)$
- cross mean: $\boldsymbol{\mu}_{ij} = \frac{\Sigma_i\boldsymbol{\mu}_j + \Sigma_j\boldsymbol{\mu}_i}{\Sigma_i + \Sigma_j}$
- cross covariance: $\Sigma_{ij} = \frac{2\Sigma_i\Sigma_j}{\Sigma_i + \Sigma_j}$
- cross time delay: $\boldsymbol{\theta}_{ij} = \boldsymbol{\theta}_i - \boldsymbol{\theta}_j$
- cross phase delay: $\phi_{ij} = \phi_i - \phi_j$

where Q is the number of auto-convolution component in the GCSM kernel, $\boldsymbol{\theta}_i$ and ϕ_i respectively denote time delay and phase delay in the i -th Gaussian spectral density. $\hat{k}_{\text{GCSM}}^{i \times j}(\mathbf{s})$ is a cross spectral density with weight w_{ij} between the i -th and j -th base Gaussians in the frequency domain.

$$\hat{k}_{\text{GCSM}}^{i \times j}(\mathbf{s}) = w_{ij} a_{ij} \frac{\exp\left(-\frac{1}{2}(\mathbf{s} - \boldsymbol{\mu}_{ij})^\top \Sigma_{ij}^{-1}(\mathbf{s} - \boldsymbol{\mu}_{ij})\right)}{\sqrt{(2\pi)^P |\Sigma_{ij}|}} \exp\left(-\pi i (\boldsymbol{\theta}_{ij} \mathbf{s} + \phi_{ij})\right) \quad (11)$$

Here $k_{\text{GCSM}}(\tau)$ satisfies the positive semi-definite condition. Through the GCSM we can model the dependency related to time and phase delay between components. In the sequel, we denote by $\text{GCSM}_{i,j}$ ($i \neq j$), the cross covariance components of Equation (10).

We combine component level dependencies related to time and phase delay and coupling correlations between tasks in order to model complicated cohesion and coupling patterns including time and phase delay not only between component but also between tasks. The GCSM kernel is used for modeling component level dependency, and the coupling coregionalization is used to discover task level nonlinear correlations. We start by using single and independent coregionalizations, and introduce the generalized convolution spectral mixture of coregionalization (GCSM-C) kernel:

$$\begin{aligned} K_{\text{GCSM-C}}(\tau) &= B \otimes K_{\text{GCSM}} \\ &= \sum_{i=1}^Q \sum_{j=1}^Q B \otimes \left[w_{ij} a_{ij} \exp\left(-\frac{1}{2}\pi^2(2\tau - \boldsymbol{\theta}_{ij})^\top \Sigma_{ij}(2\tau - \boldsymbol{\theta}_{ij})\right) \right. \\ &\quad \left. \times \cos\left(\pi \left((2\tau - \boldsymbol{\theta}_{ij})^\top \boldsymbol{\mu}_{ij} - \phi_{ij}\right)\right) \right] \end{aligned} \quad (12)$$

where $B = CC^\top$ is the coregionalization term, B is positive-definite and C is a lower triangular matrix with free form parameterization representing the degree of correlation between tasks [4], each K_{GCSM} is an $N \times N$ matrix and \otimes denotes the Kronecker product, reflecting the coregionalization properties across multiple components.

Next, if we consider also coregionalization for each base component [24], we obtain the generalized convolution spectral mixture of coupling coregionalization (GCSM-CC) kernel with the form:

$$\begin{aligned} K_{\text{GCSM-CC}}(\tau) &= \sum_{i=1}^Q \sum_{j=1}^Q B_{ij} \otimes \left[w_{ij} a_{ij} \exp\left(-\frac{1}{2}\pi^2(2\tau - \boldsymbol{\theta}_{ij})^\top \Sigma_{ij}(2\tau - \boldsymbol{\theta}_{ij})\right) \right. \\ &\quad \left. \times \cos\left(\pi \left((2\tau - \boldsymbol{\theta}_{ij})^\top \boldsymbol{\mu}_{ij} - \phi_{ij}\right)\right) \right] \end{aligned} \quad (13)$$

$$B = \{B_{ij}\}_{i=1, j=1}^Q, B_{ij} = C_i C_j^\top, C_i = \begin{bmatrix} \ell_{1,1}^i & & \cdots & 0 \\ \ell_{2,1}^i & \ell_{2,2}^i & & \\ \vdots & \vdots & \ddots & \vdots \\ \ell_{M,1}^i & \ell_{M,2}^i & \cdots & \ell_{M,M}^i \end{bmatrix} \quad (14)$$

where $\ell_{m,n}^i$ is the correlation of task m and task n in the i -th base component. Noting that C_i incorporates the degrees of correlation between tasks in the i -th component. While, $C_i C_i^\top$ is the ordinary coregionalization term, and $C_i C_j^\top$ ($i \neq j$) is the coupling coregionalization term. In addition to negative and positive correlation, time and phase shift task level correlation mentioned in MOSM [23], the proposed GCSM-CC kernel has the following desirable properties: (1) it allows to model component level dependencies including time and phase delay due to its convolution mechanism;

(2) it includes more cross components without increasing of parameter space; (3) it uses coupling coregionalization to represent task level correlation across all components; (4) it does not assume components to be independent.

The graphical representation of task level correlation and component level dependency in GCSM-CC and the others is illustrated in Figure 1.

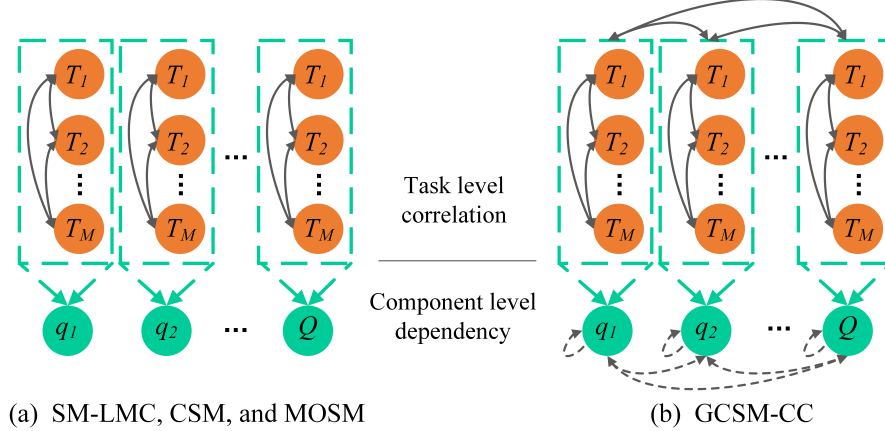


Figure 1: Comparison between GCSM-CC and the others (SM-LMC, CSM, and MOSM) in terms of task level correlation and component level dependencies. Each dashed line box contains circles (in orange) representing tasks, each connection (solid line) between circles represents a task level correlation. Each box is associated to a component (green circle): it includes all task level correlations modeled by such component. In SM-LMC, CSM, and MOSM, there are only Q components which are independent. In GCSM-CC there are Q^2 components. Each component is a convolution between two base component (component level dependency), represented by connections in dashed line.

3.2 Interpretation of component dependencies and coupling coregionalization

Channels as used in SM-LMC and CSM [21, 22] are auto-convolution of base component. SM-LMC, CSM, and MOSM treat each component independently: CSM incorporates partial phase correlations between tasks in each component, and MOSM adds task level time and phase dependency in each component. In GCSM-CC, we have as components not only auto-convolution components, but also cross convolution components, the latter ones to model dependency between component (dashed lines between base component).

Coregionalization [4, 39, 40, 41] is a powerful approach for modeling correlations among tasks. However, coregionalization was only applied to discover task correlations in single base component, and ignores coregionalization trends across multiple base components. Here we propose to use coupling coregionalization between tasks over all components, thus we have Q auto-convolution components plus $Q^2 - Q$ cross convolution components and Q auto-coregionalization plus $Q^2 - Q$ cross-coregionalization components. Note that the task auto correlation values (diagonal values of $C_i C_j^T$) are not necessarily equal to 1 because we employ the free form parameterization [4], which produces an individual scaling for each task in each component. In this way GCSM-CC can capture the coupling coregionalizations between different components. Nevertheless, GCSM-CC doesn't increase the parameter space compared to SM-LMC when no time and phase delay are considered.

Figure 2 shows cross covariances among components from time domain and its corresponding spectral densities from frequency domain. GCSM-CC is configured with $Q = 3$ base component. According to Equation (13), there are six cross covariance components ($C_i C_j, i \neq j \in \{1, 3\}$) and six coupling coregionalization terms ($C_i C_j, i \neq j \in \{1, 3\}$). The first row in Figure 2 shows only three cross covariances components (in different color solid line) because the other three components are symmetrical. The second row presents the corresponding spectral densities. From the last two rows in Figure 2, when the base component i is equal to the base component j , then the resulting coregionalizations $C_i C_i^T$'s are equivalent to those of SM-LMC and CSM. However, GCSM-CC also considers coregionalizations for $i \neq j$, hence it can represent coupling correlations between

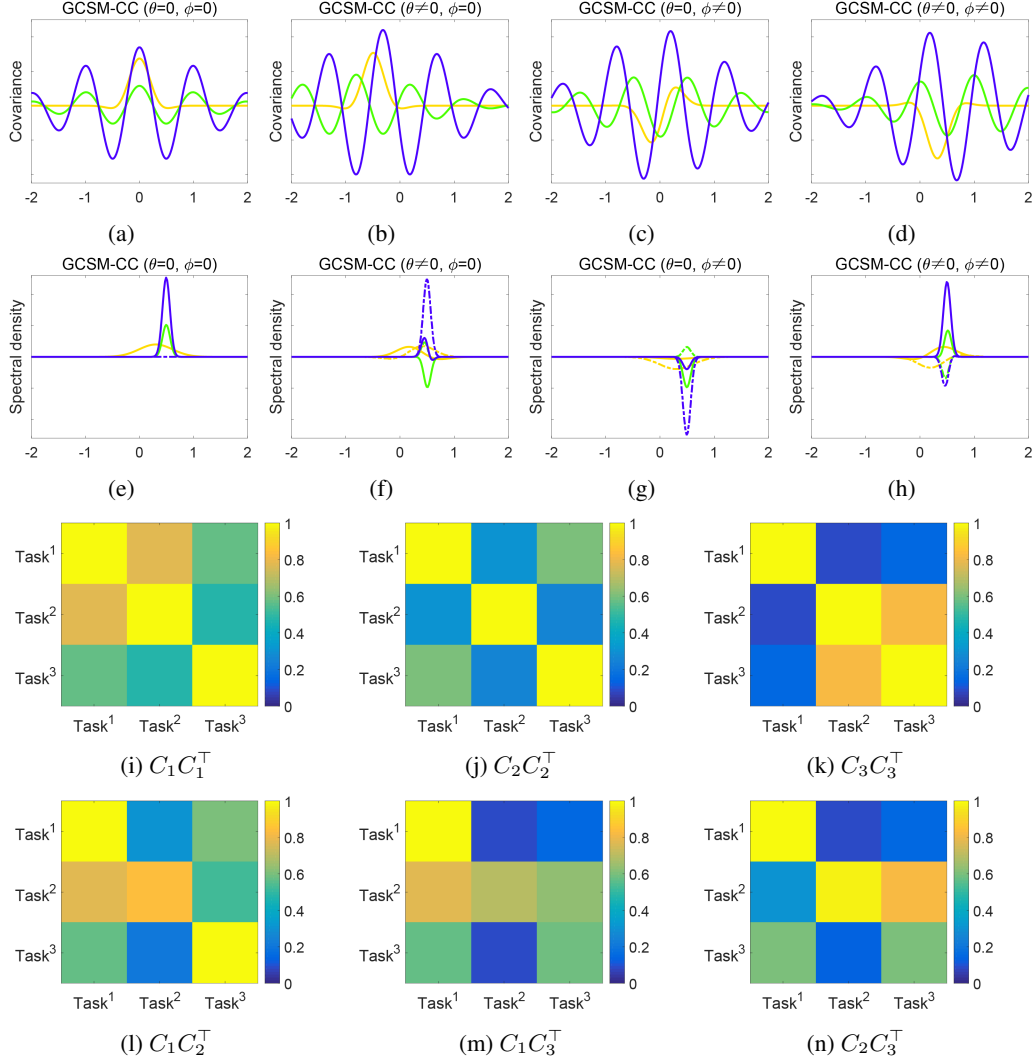


Figure 2: Cross components and corresponding spectral densities in $K_{\text{GCSM-CC}}$. First row: component level dependencies ($Q = 3$) related to zero time and phase delay, non-zero time delay and zero phase delay, zero time delay and non-zero phase delay, non-zero time and phase delay cross convolution (we only show half of 6 cross components) of GCSM-CC. Second row: corresponding spectral densities (real part in solid line and imaginary part in dashed line). Last row: coupling coregionalizations of GCSM-CC, normalized diagonal values of $C_1 C_1^\top$ in the first component (all equal to 1, since each task in the first component is assumed to be perfectly auto correlated), and normalized non diagonal values (less than 1, reflecting the correlations between tasks in the first component). $C_i C_j^\top$ represents coupling coregionalizations between component i and component j . In particular, $C_1 C_2^\top$ and $C_1 C_3^\top$, $C_2 C_3^\top$ no longer maintain symmetry, and in general their normalized diagonal values are not guaranteed to be equal to 1 because they come from different components.

tasks across all components. Moreover, these coupling coregionalizations $C_i C_j^\top$'s give task level correlations. In summary, SM-LMC provides a simple task level correlation where component are independent. CSM adds task level dependency related to phase delay. MOSM considers a more expressive task level correlation by incorporating also time delay, but still ignores component level dependencies. GCSM-CC models component level dependencies and enhances expressiveness of task level coupling correlation over all components.

3.3 Comparison with other MTGPs methods

A comparison among SM-LMC, CSM, MOSM and GCSM-CC in term of hyper-parameters, degrees of freedom and number of components is given in Table 1. Here Q denotes the number of base component and M the number of tasks.

The main difference between MOSM and GCSM-CC is that MOSM only considers task level correlation within a single component. Furthermore in MOSM, if task i is equal to task j , MOSM cannot reduce to the SM kernel.

$$k_{\text{MOSM}}(\tau) = w_i^2 (2\pi)^{\frac{n}{2}} \Sigma_i^{1/2} \exp\left(-\frac{1}{2}\tau^\top \Sigma_i \tau\right) \cos(\mu_i \tau) \quad (15)$$

GCSM-CC uses GCSM (see Introduction) and coupling coregionalization in order to model both task level correlation and component level dependency. Table 1 show characteristics of multi task kernels. SM-LMC, CSM, and GCSM-CC use free form parameterization [4]. In Table 1, θ_f and θ_ℓ are respectively length-scale and x-scale in SE and Matérn kernel. In order to make comparison more clear, we use q instead of i as a sub-index of component.

Table 1: Comparisons between multi task kernels (M tasks).

Kernel	Parameters	Degrees of freedom	Number of components
SE-LMC	$\{B, \theta_f, \theta_\ell\}$	$(M^2 + M)/2 + P + 1$	1
Matérn-LMC	$\{B, \theta_f, \theta_\ell\}$	$(M^2 + M)/2 + P + 1$	1
SM-LMC	$\{B_q, w_q, \boldsymbol{\mu}_q, \Sigma_q\}_{q=1}^Q$	$Q((M^2 + M)/2 + 2P + 1)$	Q
CSM	$\{\sigma^q, \mu^q, \{w_r^q, \phi_r^q, \phi_r^{1q} \triangleq 0\}_{r=1}^M\}_{q=1}^Q$	$2Q + M(2Q - 1)$	Q
MOSM	$\{\{w_m^q, \boldsymbol{\mu}_m^q, \Sigma_m^q, \boldsymbol{\theta}_m^q, \phi_m^q\}_{m=1}^M\}_{q=1}^Q$	$QM(3P + 2)$	Q
GCSM-C	$\{B, \{w_q, \boldsymbol{\mu}_q, \Sigma_q, \boldsymbol{\theta}_q, \phi_q\}_{q=1}^Q\}$	$(M^2 + M)/2 + Q(4P + 1)$	Q^2
GCSM-CC	$\{B_q, w_q, \boldsymbol{\mu}_q, \Sigma_q, \boldsymbol{\theta}_q, \phi_q\}_{q=1}^Q$	$Q((M^2 + M)/2 + 4P + 1)$	Q^2

4 Experiments

As other GP methods based on spectral mixture kernels, GCSM-CC is sensitive to its hyper-parameters, especially in a multi-task setting. Hyperparameters initialization has a direct impact on the ability to discover and extrapolate patterns, especially in the presence of complex multiple tasks. GCSM-CC involves more hyper-parameters than other MTGPs, namely time delay θ , phase delay ϕ and coregionalization factor C_i of each base component. Therefore we apply an initialization strategy which uses empirical spectral densities, which has been shown to be effective in other contexts [25]. However, the empirical spectral densities is often noisy, so its direct use is not possible. Past research suggested that sharp peaks of empirical spectral densities are near the true frequencies [25].

Specifically, we applied a Bayesian Gaussian mixture model $p(\Theta|\mathbf{s}) = \sum_{i=1}^Q \tilde{w}_i \mathcal{N}(\tilde{\boldsymbol{\mu}}_i, \tilde{\Sigma}_i)$ on the empirical spectral densities \mathbf{s} in order to get the Q cluster centers of Gaussian spectral densities. We use the Expectation Maximization algorithm [42] to estimate the parameters \tilde{w}_i , $\tilde{\boldsymbol{\mu}}_i$, and $\tilde{\Sigma}_i$. The results are used as initial values of w_i , $\boldsymbol{\mu}_i$, and Σ_i , respectively. Then, we randomly initialize coregionalization factors C_i 's with free-form parameterization [4] and add a positive term to make values in the diagonal of matrix C_i to be bigger than values in the rest of the matrix. We use this technique in all our experiments on artificial and real world data.

We compare GCSM-CC with existing MTGP methods, namely SM-LMC, CSM, MOSM. First we show the ability of GCSM-CC to model a mixed signal sampled from a Gaussian distribution, its integral and derivative. Then we use GCSM-CC for prediction tasks on a real-world problem with three sensor array datasets¹ related to air pollution monitoring: Nitrogen oxide (NO) concentration, Ozone concentration, and PM10 concentration extrapolating. We implemented our models in Tensorflow [43] and GPflow [44] to improve scalability and to facilitate gradient computation. The

¹<http://slb.nu/slbanalys/historiska-data-luft/>

open source codes will be made available. In all experiments we use the mean absolute error $MAE = \sum_{i=1}^n |y_i - \tilde{y}_i|/n$ as performance metric.

4.1 Synthetic experiment

We consider an artificial experiment in order to validate the interpolation, extrapolation, and signal recovery ability of GCSM-CC and compare its pattern recognition performance with that of other MTGP methods. We consider three tasks: a mixed signal, its integral, and its derivative, respectively. Specifically, we generate a Gaussian signal with length 300 in the interval $[-10, 10]$ and numerically compute its first integral and derivative.

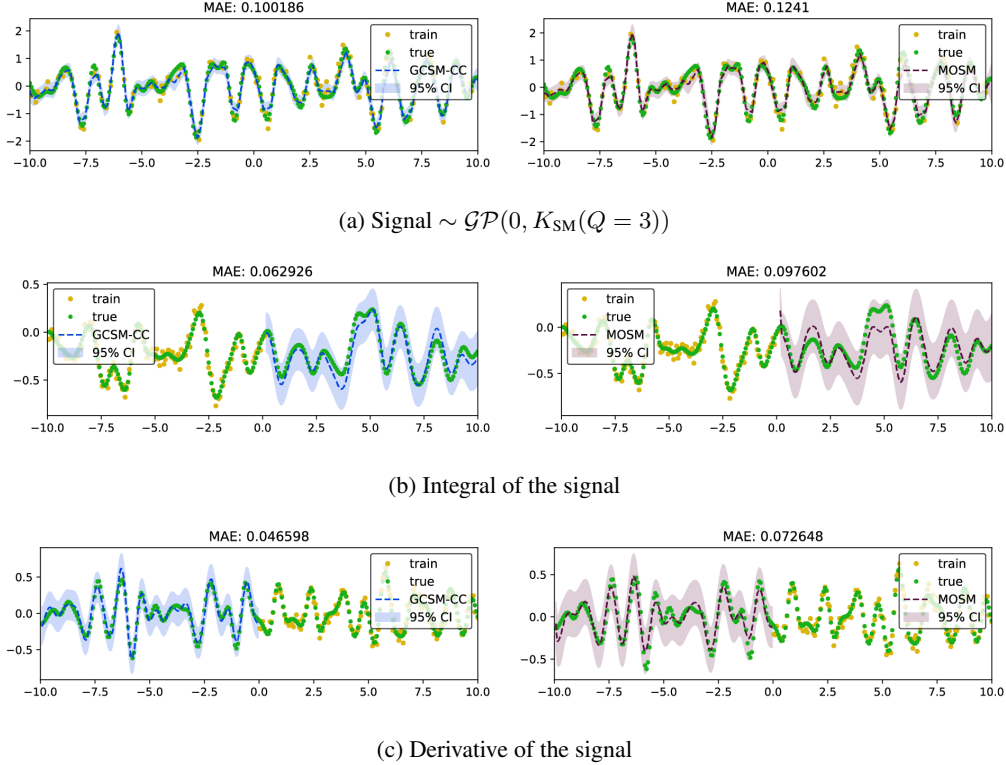


Figure 3: Performance of GCSM-CC (in blue dashed line) and MOSM (in plum dashed line) on artificial dataset. (a) Signal randomly sampled from $\mathcal{GP}(0, K_{SM})$ with $Q = 3$, training data points are randomly selected from signal and the remaining points are used as test data. (b) Integral of the signal was numerically computed, the first half of data $x \in [-10, 0]$ was selected as a training and the rest as a test. (c) Derivative of the signal was numerically computed, the last half of data $x \in [0, 10]$ was selected as a training and the rest as a test.

From a signal sampled from $\mathcal{GP}(0, K_{SM})$ we randomly choose half of data as training data, and the rest as test data. The integration signal points in the interval $[-10, 0]$ are used for training (in dark yellow), while the remaining signal points in the interval $[0, 10]$ are used for testing (in green). For the second task, the derivative of the signal in the interval $[0, 10]$ is used for training and the rest of the signal is used for testing. The performance of GCSM-CC on the generated signal is shown in Figure 3 (a). As shown in Table 2, all considered GP methods have comparable performance: they learn the covariance between tasks and interpolate well the missing values.

The second task, i.e., the integral of the signal, is shown in Figure 3 (b). In this case its inherent patterns are more difficult to recognize and extrapolate. Here GCSM-CC performs better than other methods: it achieves lowest MAE as well as smallest confidence interval. GCSM-CC excels also on the last task, i.e., the derivative signal (see Figure 3 (c)): here GCSM-CC shows best pattern learning and extrapolation capability while using the same number of base component ($Q = 10$). Predictions obtained using SE-LMC and Matérn-LMC kernels are of low quality, especially for the

extrapolating tasks (integral and derivative signals): it is very hard for them to find valid patterns in the data, like the change of trend over time. Overall, results indicate the capability of GCSM-CC to capture integration and differentiation patterns of the generated signal simultaneously.

Signal	SE-LMC	Matérn-LMC	SM-LMC	CSM	MOSM	GCSM-CC
$\mathcal{GP}(0, K_{SM})$	0.155	0.107	0.114	0.111	0.124	0.100
Integral	0.270	0.263	0.338	0.138	0.098	0.063
Derivative	0.190	0.194	0.076	0.184	0.073	0.047

Table 2: Performance (MAE) of GCSM-CC and other methods on the artificial dataset.

4.2 Nitrogen oxides (NO) concentration extrapolation

The sensor network dataset recorded from Stockholm city monitor air pollution parameters in order to provide air quality surveillance for the regional environment. In particular, Nitrogen oxides (NO) is an important parameter, since long term exposure at high concentration can cause inflammation of the human airways. Extrapolation and forecasting models allow to monitor NO concentration in order to control and prevent negative effects on health and environment. As first real world dataset, we use NO concentration from 5 January, 2017 to 25 January, 2017, in one-hour intervals, collected at three stations (Essingeleden, Hornsgatan, Sveavägen) in Stockholm and outside.

Each station corresponds to a task: Essingeleden as task 1, Hornsgatan as task 2 and Sveavägen as task 3. NO evolution shows time and phase related patterns and their variability over the period of recording. Different stations have different local patterns which depend on the station’s surroundings. For instance: Essingeleden’s measurement are recorded at open path, Hornsgatan’s measurement and Sveavägen’s measurement at street. Still, these tasks have shared global trends because of the global seasonal change and periodic characteristics of human and industry activities. The evolution of NO concentration in each task is a result of nonlinear interaction of time and phase dependent local and global patterns. Therefore data from stations should help each other when used to model long range extrapolation trends.

We aim to assess comparatively the long range extrapolation ability of GCSM-CC on future forecasting and signal recovery simultaneously. Therefore we perform extrapolation for task 2 and 3. Therefore for task 1 we randomly chose half of the Essingeleden time series as training data. For task 2 the first half of the Hornsgatan time series is used for training and the remaining data for testing. For task 3 the last half of the Sveavägen time series is used for training and the rest for testing.

We use $Q = 10$ for all methods. Hyperparameters w , σ , and μ are initialized using Gaussian mixture clustering of spectral densities in the frequency domain (see Section 4), while θ , ϕ are randomly initialized for CSM, MOSM and GCSM-CC, and the coregionalization terms in SM-LMC, CSM, GCSM-CC are also randomly initialized.

Results indicate that all SM based kernels can extrapolate the future NO concentration well, with GCSM-CC achieving better performance (see Figure 4 and Table 3). As seen in Figure 3, NO concentration patterns in the considered times series are rather irregular: we can observe the presence of multiple local and global trends containing time and phase delay, because the time at which concentration peaks appear is not periodical and its amplitude is always irregular.

4.3 Ozone concentration extrapolation

As second real world experiment we use Ozone concentration recordings in sensor networks. Ozone is another important air pollution parameter reflecting the strength of fossil fuel usage and its emission. High Ozone concentration may lead to serious environment problems, for instance photochemical smog. Moreover exposure to ozone may cause respiratory illness conditions and heart attack [45]. We consider the Ozone concentration dataset collected from three stations in Stockholm city: Torkel Knutssonsgatan’s measurement at urban background, Norr Malma’s measurement at regional background, and Hornsgatan’s measurement at street. Each of these stations corresponds to a task.

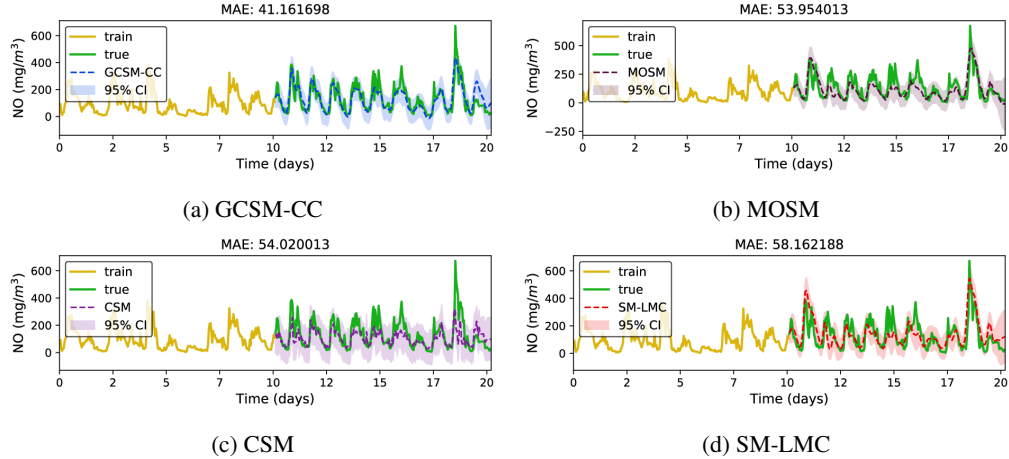


Figure 4: Nitrogen oxide (NO) concentration extrapolation task. Performance comparison between GCSM-CC and recently proposed spectral mixture kernels: (a) GCSM-CC (in blue dashed line), (b) MOSM (in plum dashed line), (c) CSM (in purple dashed line), (d) SM-LMC (in red dashed line).

We consider Ozone concentration recorded from 10 April, 2017 to 30 April, 2017. All recordings cover 24 hours at 1 hour interval. Missing values are filtered out. The change of Ozone concentration over time has a more complex trend than that of the NO concentration, because it doesn't have a stable environmental background value like NO. Similar to NO, Ozone concentration tasks are related by nonlinear interaction of local and global patterns. From Figure 5 one can also see that time and phase dependent global trends are shared across tasks. However, local patterns depend on the surrounding, which is specific to each task. The figure indicates the presence of more complicated latent patterns related to quasi-periodical human activities.

For the first task we select at random half data points of the Torkel Knutssongsgatan time series for training, for the second task the first half of the Norr Malma time series for training and the rest for testing, and for the third task the last half of the Hornsgatan time series for training and the rest for testing.

We perform extrapolation for task 2 and 3. Specifically, we use the remaining points in Norr Malma and Hornsgatan as test points to validate the long range extrapolating ability and historical signal recovery ability of GCSM-CC. We use the same hyper-parameter initialization setting as in the NO experiment. Results show that GCSM-CC consistently outperforms other kernel methods with respect to MAE and predicted confidence interval (see Figure 5 and Table 3). All methods are not fully capable to capture trends involving low concentration peaks. Nevertheless, this limitation is not crucial in this context, since for air pollution forecasting it is more important to correctly model high concentration peaks.

4.4 PM10 concentration extrapolation

The last real world experiment we consider concerns PM10 concentration recordings of sensor networks. PM10 particles have diameter smaller than 10 micrometers. They are an important air pollution parameter and are mainly produced by human activities, for example the usage of fossil fuels and power plants. PM10 forms a large proportion of air pollutants: its generation and spreading are affected by local quasi periodical industrial production and weather condition. Yearly or seasonal weather change are global factors and have a large regular variation over the year, while the variation of industrial production is a local factor and has a monthly or weekly variation. These global trends and local patterns show time and phase related variability over the period of recording. Usually for small scale variation (in 1 hour interval), the PM10 concentration depends more on its surroundings and location because human activities determine its emission. There are various time and phase dependent characteristics in the time series of this PM10 concentration experiment: short term weekly variations, medium term seasonal patterns and non-strict periodic long term trends, as well as some white noises.

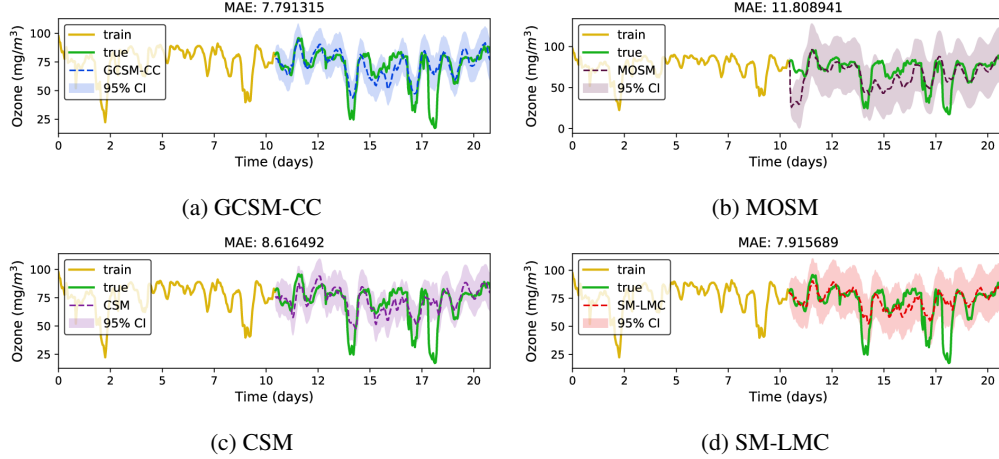


Figure 5: Ozone concentration extrapolation task. Performance comparison between GCSM and recently proposed spectral mixture kernels: (a) GCSM-CC (in blue dashed line), (b) MOSM (in plum dashed line), (c) CSM (in purple dashed line), (d) SM-LMC (in red dashed line).

The PM10 concentration dataset is collected from three stations in Stockholm city: Essingeleden’s measurement at open path (task 1), Hornsgatan’s measurement (task 2) and Sveavägen’s measurement at street (task 3). All recordings cover 24 hours at 1 hour interval. Missing values are filtered out. In this experiment, we consider PM10 concentration recording from 12 April, 2017 to 3 May, 2017. PM10 concentration over time appears to be a non-continuous signal. There are various time and phase dependent characteristics in the time series of this PM10 concentration experiment: short term weekly variations, medium term seasonal patterns and non-strict periodic long term trends, as well as white noise. The changing of PM10 concentration in the three tasks are caused by the nonlinear interaction of their time and phase related local and global patterns.

From Figure 6 one can see that the appearance of high peaks in PM10 concentration is irregular and its time of duration is short and fluctuant. Such irregular patterns are difficult to discover. Ordinary kernels cannot find any valid patterns in this dataset because of their limited expressive power. Here, we randomly choose half of PM10 concentration data points in Essingeleden, the first half of PM10 concentration data points in the Hornsgatan time series, and the last half of PM10 concentration data points in the Sveavägen time series as training data for task 1, 2, and 3, respectively. The remaining data points in Hornsgatan and Sveavägen’s time series are used for testing in order to validate the long range extrapolating and historical signal recovery ability of GCSM-CC and other MTGP methods.

Results indicate that also in this experiment GCSM-CC consistently outperforms other kernel methods at MAE, while confidence intervals are similar across methods (see Figure 6 and Table 3). In this case, high peak appearance trends are not easy to capture. GCSM-CC can forecast them well even for small sudden changes.

Signal	NO ^H	NO ^S	Ozone ^N	Ozone ^H	PM10 ^H	PM10 ^S
SE-LMC	130.960	85.063	65.554	44.271	29.813	15.156
Matérn-LMC	132.892	85.197	67.876	44.832	29.822	15.235
SM-LMC	58.162	46.809	7.916	8.911	13.505	8.461
CSM	54.020	36.000	8.616	10.826	13.794	9.406
MOSM	53.954	60.367	11.809	10.335	13.423	8.696
GCSM-CC	41.162	33.395	7.791	8.149	12.130	7.254

Table 3: Performance of kernel methods on real world datasets.

Table 3 reports the performance of the considered kernel methods on each task of the three experiments. The GCSM-CC kernel achieves the lowest MAE. Predictions using the SE-LMC and Matérn-LMC are very bad for extrapolation tasks. It is very hard for these methods to find valuable patterns in

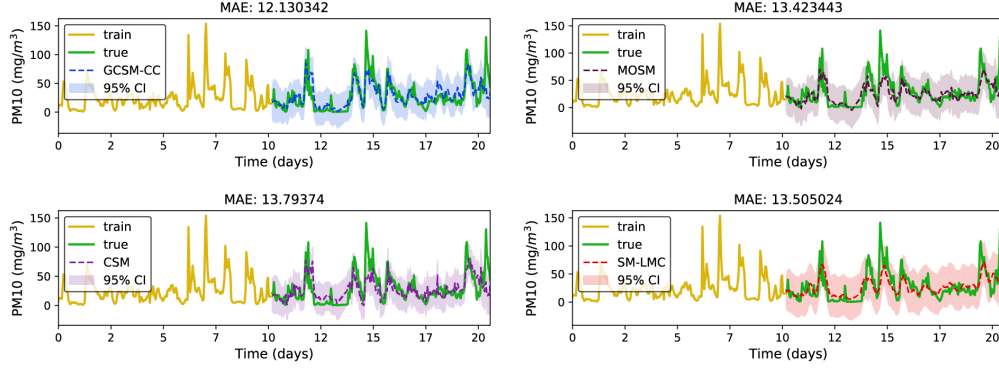


Figure 6: PM10 concentration extrapolation task. Performance comparison between GCSM-CC and recently proposed spectral mixture kernels: (a) GCSM-CC (in blue dashed line), (b) MOSM (in plum dashed line), (c) CSM (in purple dashed line), (d) SM-LMC (in red dashed line).

the data. The NO^H (NO in Hornsgatan), Ozone^N (Ozone in Norr Malma), PM10^N (PM10 in Hornsgatan) results in the table correspond to future long range extrapolating tasks, and the NO^S (NO in Sveavägen), Ozone^H (PM10 in Hornsgatan), PM10^H (PM10 in Sveavägen) results are historical long range signal recovery tasks.

5 Conclusion

We have proposed the generalized convolution spectral mixture of coupling coregionalization (GCSM-CC) kernel. The main advantages of GCSM-CC are its expressive close form, its capability to perform long range extrapolation in a multitask setting. Component dependency is modeled using the decomposition of each SM component in the frequency domain, and task level nonlinear correlations are modeled using coupling coregionalization. In this way GCSM-CC advances applicability of kernels for MTGP beyond linear correlated tasks and independent component.

Experiments on an artificial dataset and three real world datasets have shown that GCSM-CC can recognize and model component level dependent complex structures and task level nonlinear correlations, forecast at long range scale and recover long range historical signals. Like MOSM [9], a limitation of GCSM-CC is its computation complexity which is $\mathcal{O}(M^3N^3)$ (M number of tasks, N number of samples per task).

Hence GCSM-CC is M^3 times more expensive than single task GP. At present, efficient inference approximation methods like FITC and PITC [16, 17, 28, 46, 47, 48, 49, 50], are not very effective for MTGPs, because in this setting, although inducing points can still be treated as free parameters, the task label should be pre-fixed. Interesting future research involves the development of sparse and efficient inference methods for MTGPs [19, 51, 52, 53, 54]. The initialization strategy [37, 55, 56, 57] of the coupling hyperparameters C_i is also very important for multitask pattern discovery, and needs further study.

References

- [1] C. E. Rasmussen and H. Nickisch, “Gaussian processes for machine learning (gpml) toolbox,” *Journal of Machine Learning Research*, vol. 11, no. Nov, pp. 3011–3015, 2010.
- [2] C. E. Rasmussen, *Gaussian processes for machine learning*, ser. Adaptive computation and machine learning, C. K. I. Williams, Ed. Cambridge, Massachusetts: The MIT Press, 2006.
- [3] H. Liu, J. Cai, and Y.-S. Ong, “Remarks on multi-output Gaussian process regression,” *Knowledge-Based Systems*, vol. 144, pp. 102–121, 2018.
- [4] E. V. Bonilla, K. M. Chai, and C. Williams, “Multi-task Gaussian process prediction,” in *Advances in neural information processing systems*, 2008, pp. 153–160.
- [5] Z. Xu and K. Kersting, “Multi-task learning with task relations,” in *Proc. IEEE 11th Int. Conf. Data Mining*, Dec. 2011, pp. 884–893.

- [6] H. Kang and S. Choi, “Bayesian multi-task learning for common spatial patterns,” in *Proc. Int. Workshop Pattern Recognition in NeuroImaging*, May 2011, pp. 61–64.
- [7] G. Leen, J. Peltonen, and S. Kaski, “Focused multi-task learning in a Gaussian process framework,” *Machine Learning*, vol. 89, no. 1-2, pp. 157–182, 2012.
- [8] R. Dürichen, M. A. Pimentel, L. Clifton, A. Schweikard, and D. A. Clifton, “Multitask Gaussian processes for multivariate physiological time-series analysis,” *IEEE Transactions on Biomedical Engineering*, vol. 62, no. 1, pp. 314–322, 2015.
- [9] W. Ruan, A. B. Milstein, W. Blackwell, and E. L. Miller, “Multiple output Gaussian process regression algorithm for multi-frequency scattered data interpolation,” in *Proc. IEEE Int. Geoscience and Remote Sensing Symp. (IGARSS)*, Jul. 2017, pp. 3992–3995.
- [10] T. V. Nguyen and E. V. Bonilla, “Collaborative multi-output Gaussian processes,” in *Proceedings of the Thirtieth Conference on Uncertainty in Artificial Intelligence, UAI 2014, Quebec City, Quebec, Canada, July 23-27, 2014*, N. L. Zhang and J. Tian, Eds. AUAI Press, 2014, pp. 643–652. [Online]. Available: https://dslpitt.org/uai/displayArticleDetails.jsp?mmnu=1&smnu=2&article_id=2500&proceeding_id=30
- [11] H. Wackernagel, “Multivariate geostatistics, 387 pp,” 2003.
- [12] A. Melkumyan and F. Ramos, “Multi-kernel Gaussian processes,” in *IJCAI Proceedings-International Joint Conference on Artificial Intelligence*, vol. 22, no. 1, 2011, p. 1408.
- [13] I. Bilonis and N. Zabararas, “Multi-output local Gaussian process regression: applications to uncertainty quantification,” *Journal of Computational Physics*, vol. 231, no. 17, pp. 5718–5746, 2012.
- [14] B. Zhang, B. A. Konomi, H. Sang, G. Karagiannis, and G. Lin, “Full scale multi-output Gaussian process emulator with nonseparable auto-covariance functions,” *Journal of Computational Physics*, vol. 300, pp. 623–642, 2015.
- [15] P. Goovaerts, “Geostatistics for natural resources evaluation. oxford univ. press, new york.” *Geostatistics for natural resources evaluation. Oxford Univ. Press, New York.*, 1997.
- [16] M. Alvarez and N. D. Lawrence, “Sparse convolved Gaussian processes for multi-output regression,” in *Advances in neural information processing systems*, 2009, pp. 57–64.
- [17] M. A. Álvarez and N. D. Lawrence, “Computationally efficient convolved multiple output Gaussian processes,” *Journal of Machine Learning Research*, vol. 12, no. May, pp. 1459–1500, 2011.
- [18] S. Gómez-González, M. A. Álvarez, H. F. García, J. I. Ríos, and A. A. Orozco, “Discriminative training for convolved multiple-output Gaussian processes,” in *Iberoamerican Congress on Pattern Recognition*. Springer, 2015, pp. 595–602.
- [19] C. Guarnizo and M. A. Álvarez, “Fast kernel approximations for latent force models and convolved multiple-output Gaussian processes,” *arXiv preprint arXiv:1805.07460*, 2018.
- [20] A. G. Wilson, “Covariance kernels for fast automatic pattern discovery and extrapolation with Gaussian processes,” *University of Cambridge*, 2014.
- [21] A. G. Wilson, D. A. Knowles, and Z. Ghahramani, “Gaussian process regression networks,” *arXiv preprint arXiv:1110.4411*, 2011.
- [22] K. R. Ulrich, D. E. Carlson, K. Dzirasa, and L. Carin, “GP kernels for cross-spectrum analysis,” in *Advances in neural information processing systems*, 2015, pp. 1999–2007.
- [23] G. Parra and F. Tobar, “Spectral mixture kernels for multi-output Gaussian processes,” in *Advances in Neural Information Processing Systems*, 2017, pp. 6684–6693.
- [24] K. Chen, P. Groot, J. Chen, and E. Marchiori, “Spectral Mixture Kernels with Time and Phase Delay Dependencies,” *ArXiv e-prints*, Aug. 2018.
- [25] A. Wilson and R. Adams, “Gaussian process kernels for pattern discovery and extrapolation,” in *Proceedings of the 30th International Conference on Machine Learning (ICML-13)*, 2013, pp. 1067–1075.
- [26] S. Bochner, *Lectures on Fourier Integrals.(AM-42)*. Princeton University Press, 2016, vol. 42.
- [27] M. Stein, “Interpolation of spatial data: some theory for kriging. 1999.”

- [28] Y. Wang and R. Kharon, “Sparse Gaussian processes for multi-task learning,” in *Joint European Conference on Machine Learning and Knowledge Discovery in Databases*. Springer, 2012, pp. 711–727.
- [29] S. Vasudevan, A. Melkumyan, and S. Scheduling, “Information fusion in multi-task Gaussian process models,” in *Proc. IEEE Int. Conf. Multisensor Fusion and Integration for Intelligent Systems (MFI)*, Sep. 2012, pp. 225–232.
- [30] I. Bilonis, N. Zabararas, B. A. Konomi, and G. Lin, “Multi-output separable Gaussian process: towards an efficient, fully Bayesian paradigm for uncertainty quantification,” *Journal of Computational Physics*, vol. 241, pp. 212–239, 2013.
- [31] R. Dürichen, M. A. F. Pimentel, L. Clifton, A. Schweikard, and D. A. Clifton, “Multi-task Gaussian process models for biomedical applications,” in *Proc. IEEE-EMBS Int. Conf. Biomedical and Health Informatics (BHI)*, Jun. 2014, pp. 492–495.
- [32] J. Requeima, W. Tebbutt, W. Bruinsma, and R. E. Turner, “The Gaussian process autoregressive regression model (gpar),” *arXiv preprint arXiv:1802.07182*, 2018.
- [33] A. G. Wilson, E. Gilboa, A. Nehorai, and J. P. Cunningham, “Fast kernel learning for multidimensional pattern extrapolation,” in *Advances in Neural Information Processing Systems*, 2014, pp. 3626–3634.
- [34] D. Duvenaud, J. R. Lloyd, R. Grosse, J. B. Tenenbaum, and Z. Ghahramani, “Structure discovery in nonparametric regression through compositional kernel search,” *arXiv preprint arXiv:1302.4922*, 2013.
- [35] S. Flaxman, A. Wilson, D. Neill, H. Nickisch, and A. Smola, “Fast kronecker inference in Gaussian processes with non-gaussian likelihoods,” in *International Conference on Machine Learning*, 2015, pp. 607–616.
- [36] J. B. Oliva, A. Dubey, A. G. Wilson, B. Póczos, J. Schneider, and E. P. Xing, “Bayesian nonparametric kernel-learning,” in *Artificial Intelligence and Statistics*, 2016, pp. 1078–1086.
- [37] P. A. Jang, A. Loeb, M. Davidow, and A. G. Wilson, “Scalable Levy process priors for spectral kernel learning,” in *Advances in Neural Information Processing Systems*, 2017, pp. 3943–3952.
- [38] S. Remes, M. Heinonen, and S. Kaski, “A mutually-dependent hadamard kernel for modelling latent variable couplings,” in *Asian Conference on Machine Learning*, 2017, pp. 455–470.
- [39] K. Yu, V. Tresp, and A. Schwaighofer, “Learning Gaussian processes from multiple tasks,” in *Proceedings of the 22nd international conference on Machine learning*. ACM, 2005, pp. 1012–1019.
- [40] E. V. Bonilla, F. V. Agakov, and C. K. Williams, “Kernel multi-task learning using task-specific features,” in *Artificial Intelligence and Statistics*, 2007, pp. 43–50.
- [41] Y. Zhang and D.-Y. Yeung, “A convex formulation for learning task relationships in multi-task learning,” *arXiv preprint arXiv:1203.3536*, 2012.
- [42] T. K. Moon, “The expectation-maximization algorithm,” *IEEE Signal Processing Magazine*, vol. 13, no. 6, pp. 47–60, 1997.
- [43] M. Abadi, P. Barham, J. Chen, Z. Chen, A. Davis, J. Dean, M. Devin, S. Ghemawat, G. Irving, M. Isard *et al.*, “Tensorflow: A system for large-scale machine learning. arxiv preprint,” *arXiv preprint arXiv:1605.08695*, 2016.
- [44] A. G. d. G. Matthews, M. van der Wilk, T. Nickson, K. Fujii, A. Boukouvalas, P. León-Villagrà, Z. Ghahramani, and J. Hensman, “GPflow: A Gaussian process library using tensorflow,” *Journal of Machine Learning Research*, vol. 18, no. 40, pp. 1–6, 2017.
- [45] M. Jerrett, R. T. Burnett, C. A. Pope III, K. Ito, G. Thurston, D. Krewski, Y. Shi, E. Calle, and M. Thun, “Long-term ozone exposure and mortality,” *New England Journal of Medicine*, vol. 360, no. 11, pp. 1085–1095, 2009.
- [46] M. Álvarez, D. Luengo, M. Titsias, and N. Lawrence, “Efficient multioutput Gaussian processes through variational inducing kernels,” in *Proceedings of the Thirteenth International Conference on Artificial Intelligence and Statistics*, 2010, pp. 25–32.
- [47] C. K. Williams and M. Seeger, “Using the nystrom method to speed up kernel machines,” in *Advances in neural information processing systems*, 2001, pp. 682–688.

- [48] J. Quiñero-Candela and C. E. Rasmussen, “A unifying view of sparse approximate Gaussian process regression,” *Journal of Machine Learning Research*, vol. 6, no. Dec, pp. 1939–1959, 2005.
- [49] E. Snelson and Z. Ghahramani, “Sparse Gaussian processes using pseudo-inputs,” in *Advances in neural information processing systems*, 2006, pp. 1257–1264.
- [50] K. Chalupka, C. K. Williams, and I. Murray, “A framework for evaluating approximation methods for Gaussian process regression,” *Journal of Machine Learning Research*, vol. 14, no. Feb, pp. 333–350, 2013.
- [51] B. Rakitsch, C. Lippert, K. Borgwardt, and O. Stegle, “It is all in the noise: Efficient multi-task Gaussian process inference with structured residuals,” in *Advances in neural information processing systems*, 2013, pp. 1466–1474.
- [52] H. Soleimani, J. Hensman, and S. Saria, “Scalable joint models for reliable uncertainty-aware event prediction,” *IEEE transactions on pattern analysis and machine intelligence*, 2017.
- [53] J. R. Gardner, G. Pleiss, R. Wu, K. Q. Weinberger, and A. G. Wilson, “Product kernel interpolation for scalable Gaussian processes,” *arXiv preprint arXiv:1802.08903*, 2018.
- [54] H. Liu, Y.-S. Ong, X. Shen, and J. Cai, “When Gaussian process meets big data: A review of scalable gps,” *arXiv preprint arXiv:1807.01065*, 2018.
- [55] K. Swersky, J. Snoek, and R. P. Adams, “Multi-task Bayesian optimization,” in *Advances in neural information processing systems*, 2013, pp. 2004–2012.
- [56] R. Martinez-Cantin, “Bayesopt: A Bayesian optimization library for nonlinear optimization, experimental design and bandits,” *The Journal of Machine Learning Research*, vol. 15, no. 1, pp. 3735–3739, 2014.
- [57] N. Knudde, J. van der Herten, T. Dhaene, and I. Couckuyt, “GPflowopt: A Bayesian optimization library using tensorflow,” *arXiv preprint arXiv:1711.03845*, 2017.